Electronic Supplementary Material (ESI) for Inorganic Chemistry Frontiers.

Supporting Information

Steering visible-light-driven photocatalytic activity by forming $LaTaON_2$-$BaTaO_2N$ solid solutions for water oxidation into oxygen

Yuwei Zhang [a] and Xiaoxiang Xu[a,*]

[a] *Shanghai Key Lab of Chemical Assessment and Sustainability, School of Chemical Science and Engineering, Clinical and Central Lab, Putuo People's Hospital, Tongji University, Shanghai, China Address here. Email: xxxu@tongji.edu.cn, telephone: +86-21-65986919*

Corresponding author

Xiaoxiang Xu (Email: xxxu@tongji.edu.cn; Tel: +86-021-65986919)

Supporting information content

Number of pages: 19 (S1-S19)

Number of figures: 11 (Figure S1 to S11)

Number of tables: 7 (Table S1 to S7)

Content

Figure:

Tables:

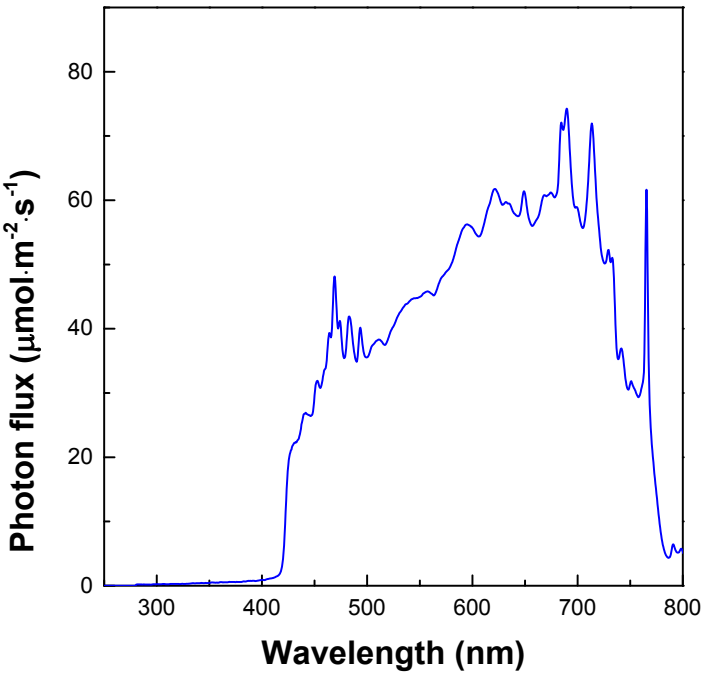

Figure S1. Spectra of Xenon lamp coupled with a cut-off filter ($\lambda \geq 420$ nm).

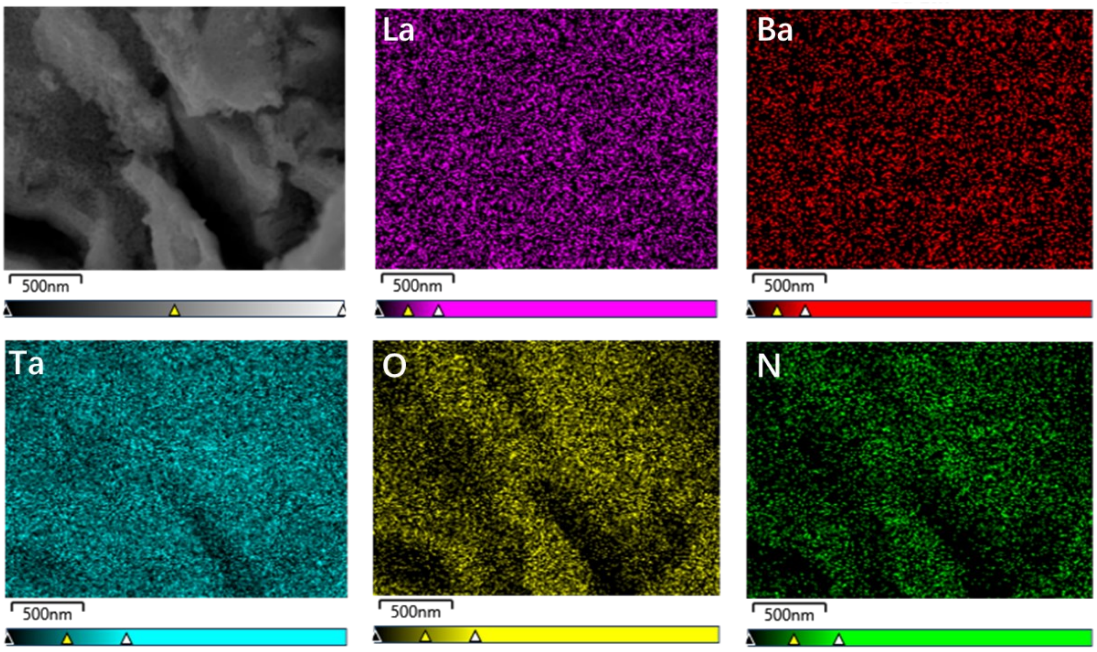

Figure S2. SEM-EDX mapping of sample $La_{0.2}Ba_{0.8}TaO_{y+1}N_{2-y}$ (x = 0.8).

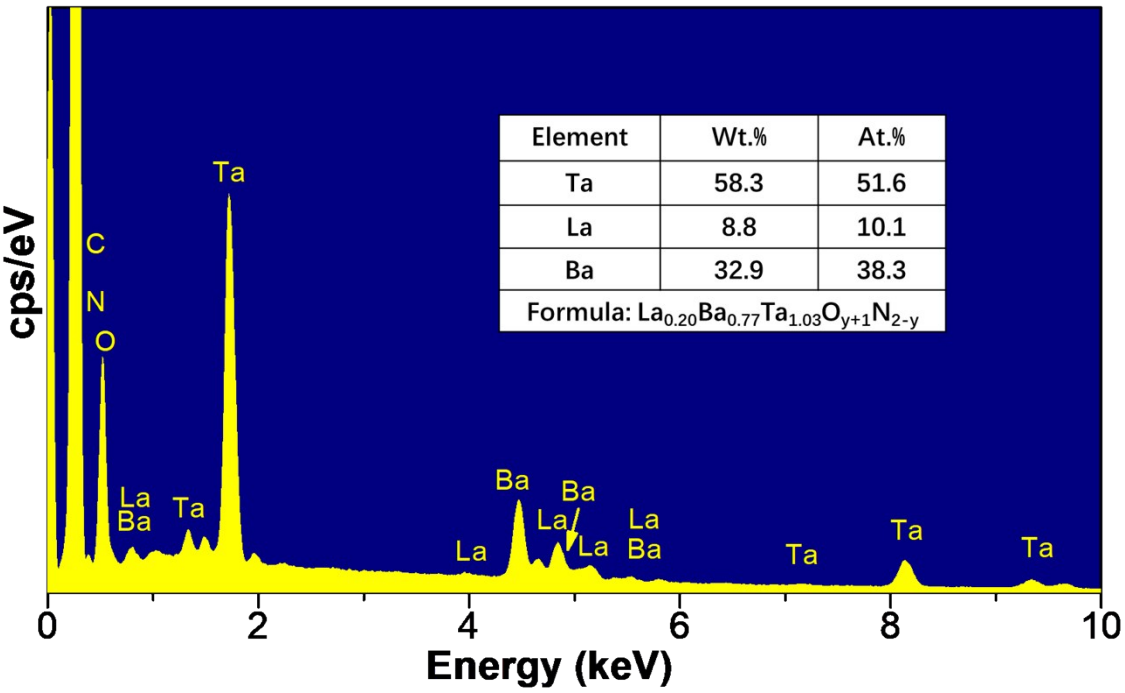

Figure S3. SEM-EDX element analysis of sample $La_{0.2}Ba_{0.8}TaO_{y+1}N_{2-y}$ (x = 0.8).

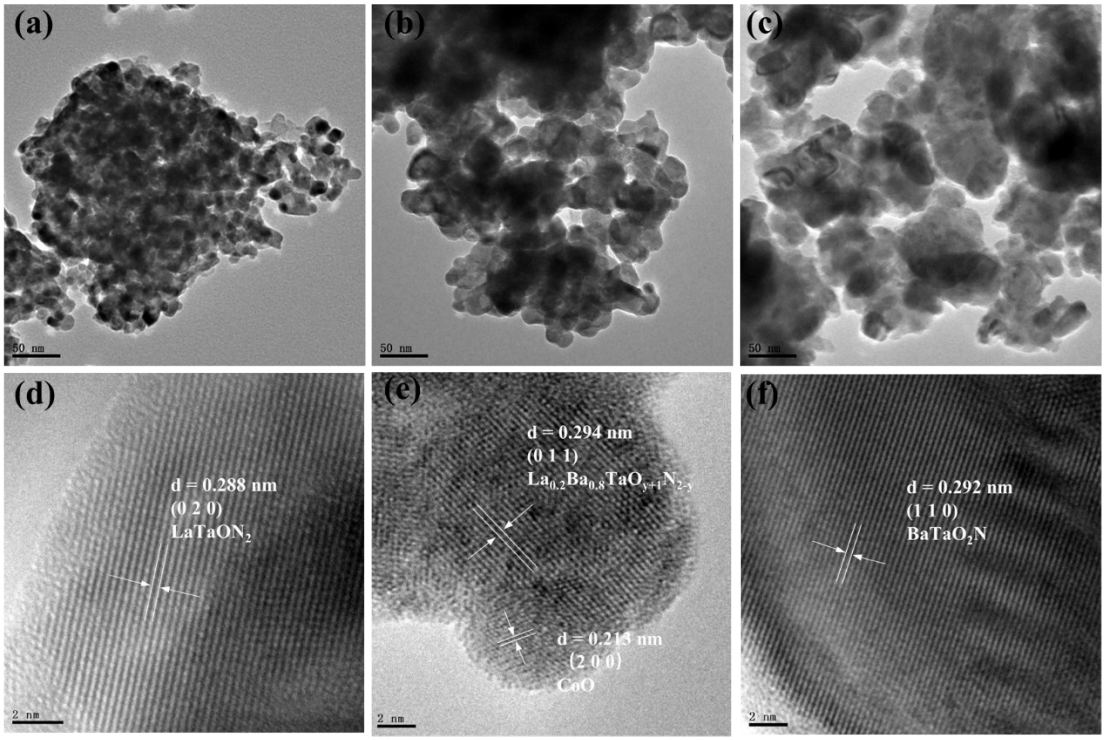

Figure S4. Transmission electron microscopy (TEM) and high-resolution transmission electron microscopy (HRTEM) images of (a, d) $LaTaON_2$ (x = 0.0), (b, e) $La_{0.2}Ba_{0.8}TaO_{y+1}N_{2-y}$ (x = 0.8) and (c, f) $BaTaO_2N$ (x = 1.0).

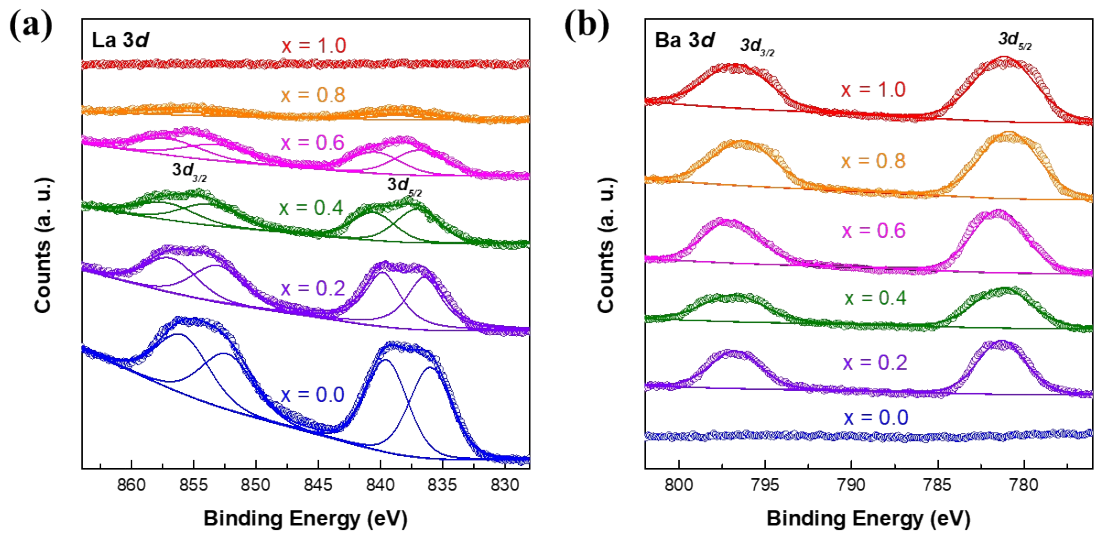

Figure S5. X-ray photoelectron spectra of sample $La_{1-x}Ba_xTaO_{y+1}N_{2-y}$ ($0 \leq x, y \leq 1$): (a) La 3*d* state; (b) Ba 3*d* state.

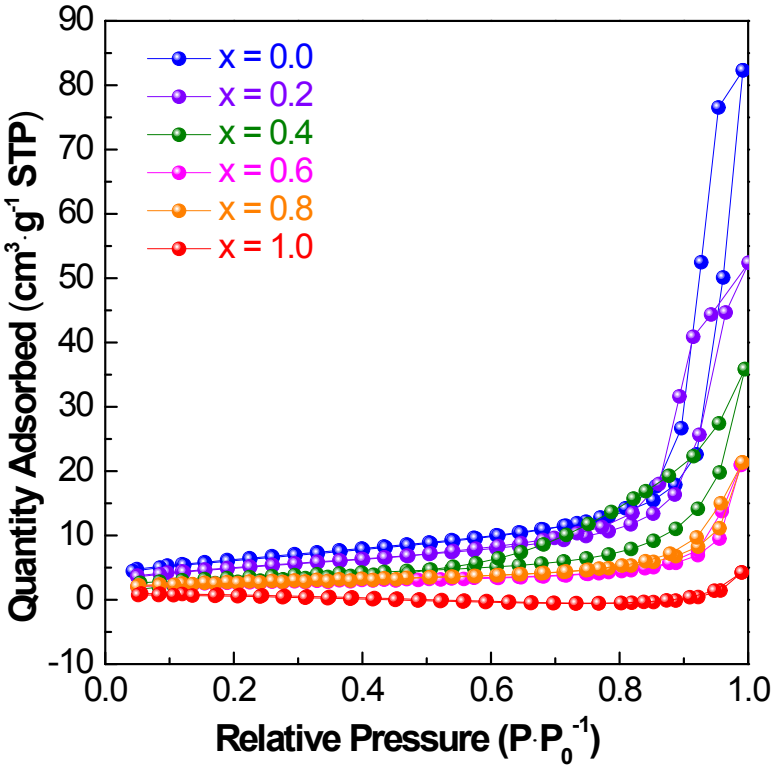

Figure S6. Nitrogen adsorption-desorption isotherms of freshly prepared sample powder $La_{1-x}Ba_xTaO_{y+1}N_{2-y}$ ($0 \leq x, y \leq 1$), the calculated BET surface area and FWHM of XRD are tabulated on table S2.

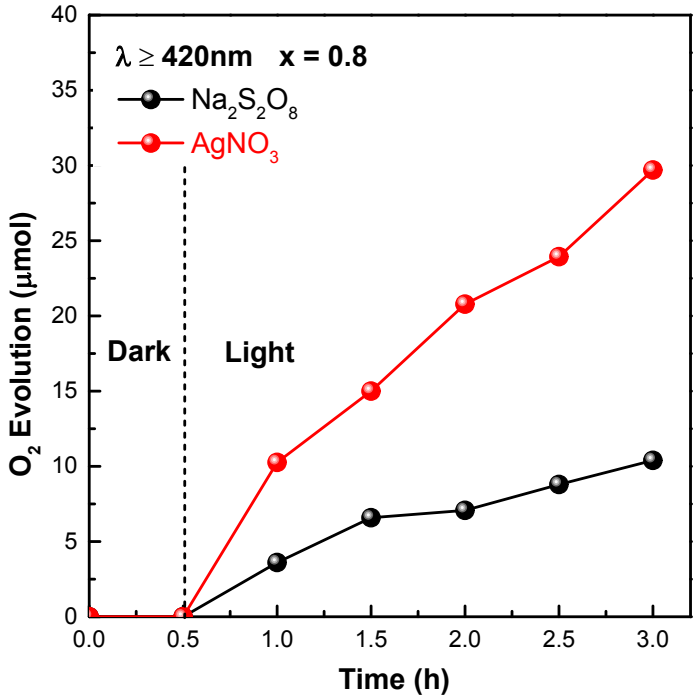

Figure S7. Photocatalytic oxygen evolution for $La_{0.2}Ba_{0.8}TaO_{y+1}N_{2-y}$ (x = 0.8) loaded with 2 wt% CoO_x under visible light illumination ($\lambda \geq 420$ nm), sodium persulfate (0.05 M) or silver nitrate aqueous solution (0.05 M) was used as a sacrificial agent.

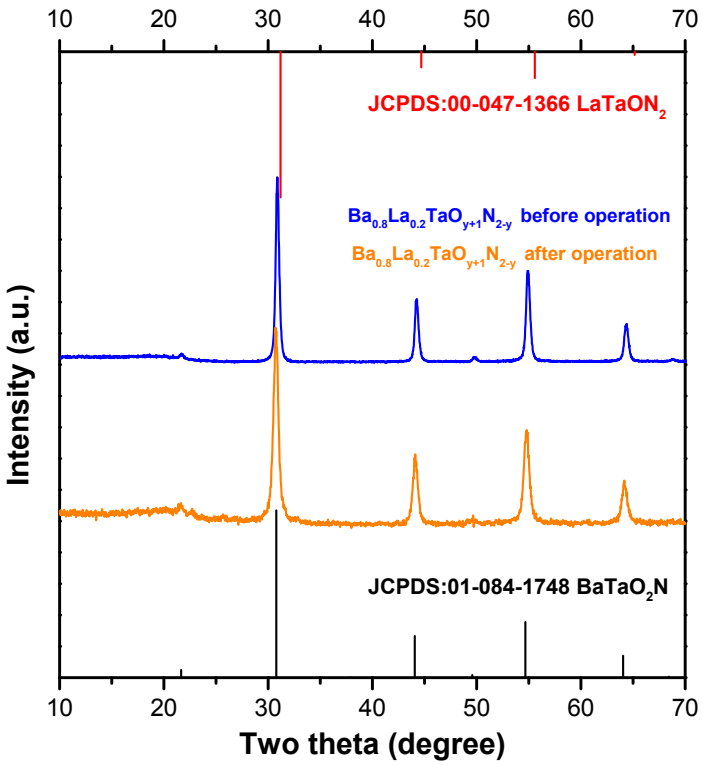

Figure S8. XRD pattern of $La_{0.2}Ba_{0.8}TaO_{y+1}N_{2-y}$ (x = 0.8) before and after oxidation treatment.

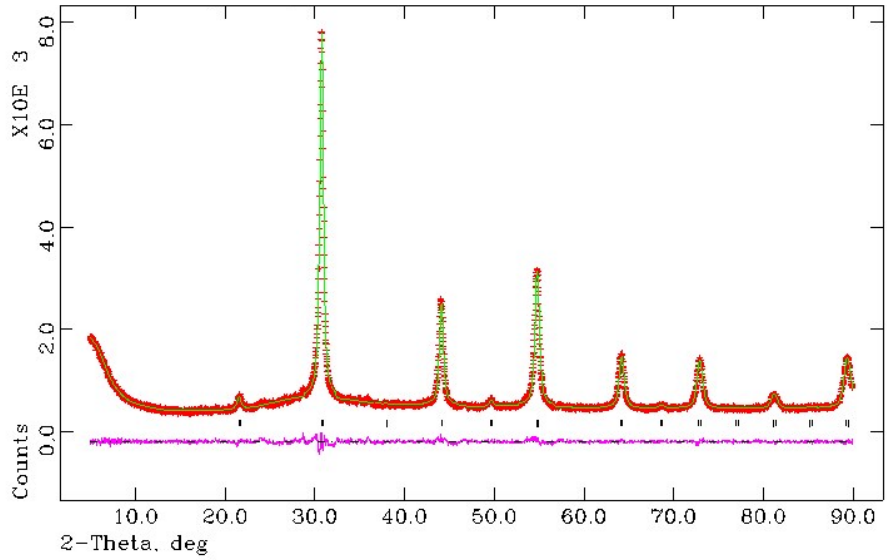

Figure S9. Observed and calculated XRD pattern of $La_{0.2}Ba_{0.8}TaO_{y+1}N_{2-y}$ (x = 0.8) after photocatalytic experiment (R_p = 4.05%, R_{wp} = 3.10%, χ^2 = 1.085).

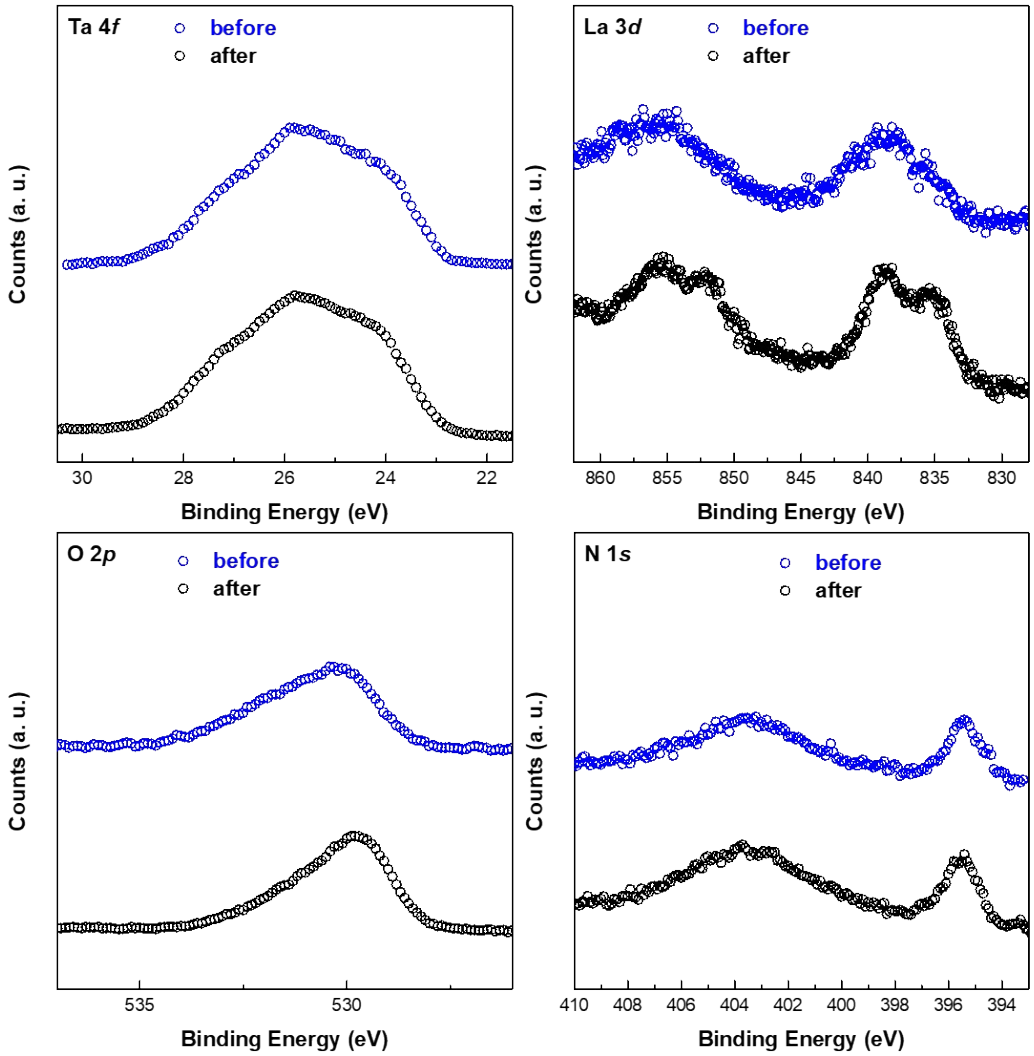

Figure S10. X-ray photoelectron spectra of $La_{0.2}Ba_{0.8}TaO_{y+1}N_{2-y}$ (x = 0.8) before and after photocatalytic experiment.

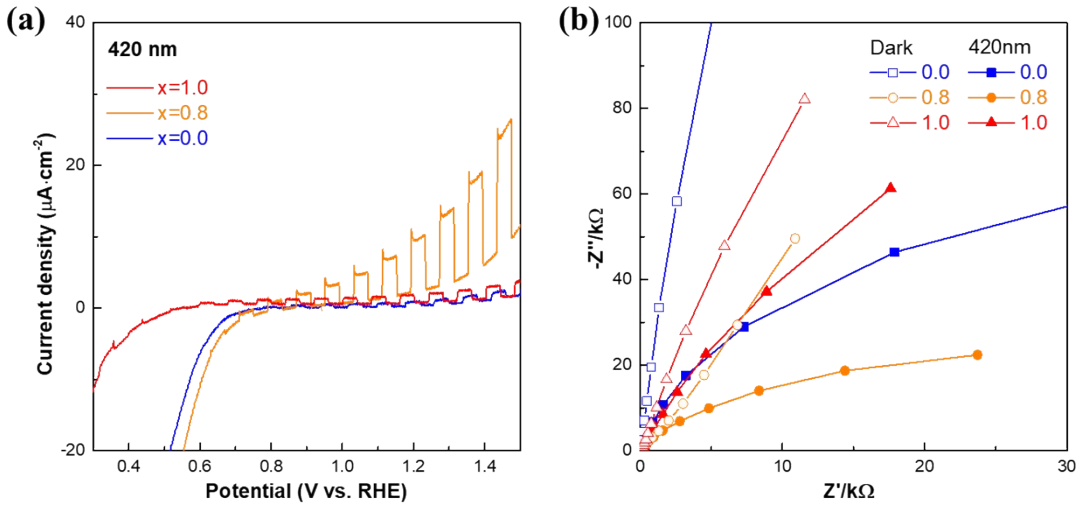

Figure S11. (a) Linear sweep voltammetry (LSV) and (b) impedance spectra for photoelectrode fabricated from samples $LaTaON_2$ (x = 0.0), $La_{0.2}Ba_{0.8}TaO_{y+1}N_{2-y}$ (x = 0.8) and $BaTaO_2N$ (x = 1.0).

Table S1. BET surface area and FWHM of samples $La_{1-x}Ba_xTaO_{y+1}N_{2-y}$ ($0 \leq x, y \leq 1$).

x	BET surface area （m²/g）	FWHM of main peak （°）
0.0	22.1	1.2
0.2	17.8	1.1
0.4	12.0	1.1
0.6	8.9	0.9
0.8	9.3	0.5
1.0	1.8	0.2

Table S2. Element content from oxygen and nitrogen analysis and the deduced chemical formula

x	O content (wt.%)	N content (wt.%)	Chemical formula
0.8	9.1	7.2	$La_{0.2}Ba_{0.8}TaO_{1.67}N_{1.33}$

Table S3. XPS data on the peak fitting analysis for Ta 4*f*

x	Element state	FWHM (eV)	Position (eV)	Area	Position (eV)	Area
0.0	Ta^{4+}	1.25	26.07	26894.76	24.17	35859.68
	Ta^{5+}	1.86	27.25	30463.74	25.35	40618.32
0.2	Ta^{4+}	1.32	26.12	24346.02	24.22	32461.36
	Ta^{5+}	1.60	27.44	27272.83	25.54	36363.77
0.4	Ta^{4+}	1.33	26.10	11946.99	24.20	15929.32
	Ta^{5+}	1.86	27.29	22989.45	25.39	30652.60
0.6	Ta^{4+}	1.35	26.17	19934.93	24.27	26579.91
	Ta^{5+}	1.65	27.38	30959.82	25.48	41279.77
0.8	Ta^{4+}	1.21	26.15	8734.036	24.25	11645.38
	Ta^{5+}	1.87	27.31	21443.53	25.41	28591.37
1.0	Ta^{4+}	1.21	26.32	6102.065	24.42	8136.086
	Ta^{5+}	1.85	27.40	18954.80	25.50	25273.07

Table S4. Peak positions on XPS analysis for La, Ba, Ta, O and N

Element state	Peak position (eV)	Element state	Peak position (eV)
La^{3+}	836.5 ($3d_{5/2}$)	Ta^{4+}	24.3 ($4f_{7/2}$)
La^{3+}	839.8 ($3d_{5/2}$)	Ta^{4+}	26.2 ($4f_{5/2}$)
La^{3+}	853.0 ($3d_{3/2}$)	Ta^{5+}	25.4 ($4f_{7/2}$)
La^{3+}	856.9 ($3d_{3/2}$)	Ta^{5+}	27.3 ($4f_{5/2}$)
Ba^{2+}	796.7 ($3d_{3/2}$)	OH^{-}	531.6 ($2p$)
Ba^{2+}	781.3 ($3d_{5/2}$)	O^{2-}	529.7 ($2p$)
N^{3-}	395.6 ($1s$)		

Table S5. Unit parameters for $La_{0.2}Ba_{0.8}TaO_{y+1}N_{2-y}$ (x = 0.8) after photocatalytic experiment, standard deviation is included in the parenthesis.

x	Space group	a (Å)	b (Å)	c (Å)	β (°)	B.L. (Å)	A (°)	V (Å^3)
0.8	$Pm\bar{3}m$	4.1035(1)	4.1035(1)	4.1035(1)	90	2.0518(1)	180	69.099(2)

Table S6. O_2 evolution of some typical oxynitride and non-oxynitride photocatalysts under visible light illumination ($\lambda \geq 420$ nm)

Photocatalyst	Co-catalyst	O_2 (μmol h^{-1})	Ref.
$LaTaON_2$	-	5.0	1
$SrTaO_2N$	2 wt% CoO_x	22.5	2
$CaTaO_2N$	-	2.9	3
$BaNbO_2N$	2 wt% CoO_x	15.3	4
$RbPb_2Nb_3O_{10}$	-	1.3	5
WO_3	PtO_x	24.0	6
$BiVO_4$	-	15.0	7

Table S7. Photocurrent densities (1.23 V vs. RHE) of $La_{0.2}Ba_{0.8}TaO_{y+1}N_{2-y}$ (x = 0.8) compared with other compounds under visible light illumination ($\lambda \geq 420$ nm)

Photocatalyst	photocurrent density (μA)	Ref.
$La_{0.2}Ba_{0.8}TaO_{y+1}N_{2-y}$	10.4	Our work
$LaTaON_2$	2.3	8
$CaTaO_2N$	9.2	9
$CuWO_4$	~200	10
$SrTaO_2N$	8.6	11

Reference

1 L. Zhang, Y. Song, J. Feng, T. Fang, Y. Zhong, Z. Li, Z. Zou, Photoelectrochemical water oxidation of $LaTaON_2$ under visible-light irradiation, International Journal of Hydrogen Energy, 2014, 39, 7697-7704.

2 J. Fu, S.E. Skrabalak, Enhanced Photoactivity from Single-Crystalline $SrTaO_2N$ Nanoplates Synthesized by Topotactic Nitridation, Angewandte Chemie-International Edition, 2017, 56, 14169-14173.

3 J. Xu, C. Pan, T. Takata, K. Domen, Photocatalytic overall water splitting on the perovskite-type transition metal oxynitride $CaTaO_2N$ under visible light irradiation, Chemical Communications, 2015, 51, 7191-7194.

4 B. Siritanaratkul, K. Maeda, T. Hisatomi, K. Domen, Synthesis and Photocatalytic Activity of Perovskite Niobium Oxynitrides with Wide Visible-Light Absorption Bands, ChemSusChem, 2011, 4, 74-78.

5 J. Yoshimura, Y. Ebina, J. Kondo, K. Domen, A. Tanaka, Visible-light induced photocatalytic behavior of a layered perovskite type niobate $RbPb_2Nb_3O_{10}$, Journal of Physical Chemistry, 1993, 97, 1970-1973.

6 O. Tomita, S. Nitta, Y. Matsuta, S. Hosokawa, M. Higashi, R. Abe, Improved Photocatalytic Water Oxidation with Fe^{3+}/Fe^{2+} Redox on Rectangular-shaped WO_3 Particles with Specifically Exposed Crystal Faces via Hydrothermal Synthesis, Chemistry Letters, 2016, 46, 221-224.

7 W. Yao, J. Ye, A new efficient visible-light-driven photocatalyst $Na_{0.5}Bi_{1.5}VMoO_8$ for oxygen evolution, Chemical Physics Letters, 2008,450, 370-374.

8 Y. Wang, S. Jin, G. Pan, Z. Li, L. Chen, G. Liu, X. Xu, Zr doped mesoporous $LaTaON_2$ for efficient photocatalytic water splitting, Journal of Materials Chemistry A, 2019, 7, 5702-5711.

9 Y. Wang, S. Wei, X. Xu, $SrTaO_2N$-$CaTaO_2N$ solid solutions as efficient visible light active photocatalysts for water oxidation and reduction, Applied Catalysis B-Environmental, 2020,263.

10 P. Shadabipour, A.L. Raithel, T.W. Hamann, Charge-Carrier Dynamics at the $CuWO_4$/Electrocatalyst Interface for Photoelectrochemical Water Oxidation, Acs Applied Materials & Interfaces, 2020, 12, 50592-50599.

11 Z. Ma, K. Pietak, J. Piatek, J. R. DeMoulpied, A. Rokicinska, P. Kustrowski, R. Dronskowski, S. Zlotnik, R. H. Coridan and A. Slabon, Semi-transparent quaternary oxynitride photoanodes on GaN underlayers, Chemical Communications, 2020, 56, 13193-13196.